MATER. RES. LETT.
2019, VOL. 7, NO. 6, 251–257
https://doi.org/10.1080/21663831.2019.1595763

MATERIALS RESEARCH LETTERS
Taylor & Francis
Taylor & Francis Group

ORIGINAL REPORT

Strong and ductile beta Ti–18Zr–13Mo alloy with multimodal twinning

Jinyong Zhang[a,b,c], Fan Sun[d], Zheng Chen[a], Yang Yang[e], Baolong Shen[a], Ju Li[e] and Frédéric Prima[d]

[a]School of Material Science and Engineering, China University of Mining and Technology, Xuzhou, People's Republic of China; [b]Center for Advancing Materials Performance from the Nanoscale (CAMP-Nano), State Key Laboratory for Mechanical Behavior of Materials, Xi'an Jiaotong University, Xi'an, People's Republic of China; [c]State Key Laboratory of Materials Processing and Die & Mould Technology, Huazhong University of Science and Technology, Wuhan, People's Republic of China; [d]PSL Research University, Chimie ParisTech-CNRS, Institut de Recherche de Chimie Paris, Paris, France; [e]Department of Nuclear Science and Engineering and Department of Materials Science and Engineering, Massachusetts Institute of Technology, Cambridge, MA, USA

ABSTRACT

Body-centred cubic (BCC) Ti–18Zr–13Mo (wt%) alloy displays excellent yield strength ($\approx$ 800 MPa), stable hardening (rate $>$ 1500 MPa) and uniform ductility $>$ 18%, resulting from multi-TWIP (multiple twinning-induced plasticity) strengthening effect. This multimodal mechanisms include micro-scale $\{332\}<113>$ deformation twinning (DT), nano-scale $\{112\}<111>$ DT and a rare $\{5\ 8\ 11\}<135>$ DT mode. Martensitic phase transformation is completely suppressed and the sample stays a single-phase solid solution throughout the deformation. *In situ* electron backscatter diffraction (EBSD) and transmission electron microscopy (TEM) were used to characterize the multi-TWIP and dynamic Hall–Patch effect, with dislocation slip and large grain distortions at twin interfaces.

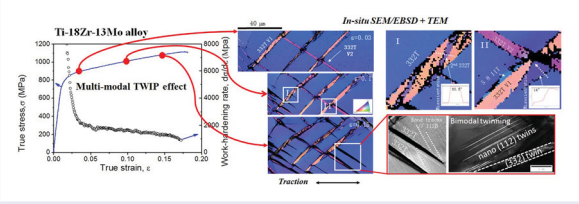

ARTICLE HISTORY
Received 3 December 2018

KEYWORDS
Vacuum arc-melting beta Ti; deformation mechanisms; twinning; multimodal TWIP

IMPACT STATEMENT

The addition of Zr solutes stabilizes β Ti-alloy and completely suppresses phase transformations, allowing $\{332\}<113>$, $\{112\}<111>$ and $\{5\ 8\ 11\}<135>$ multimodal twinning to give a better combination of strength, strain-hardening rate and ductility.

Titanium alloys are attractive for aerospace, orthopaedic implants and sporting goods industries and automotive applications thanks to their low density, high strength, non-magnetic, good hardenability, and good corrosion resistance [1]. In the β Ti-alloys, the β phase stability during deformation is often called into question. It has been reported [1,2] that the deformation mechanism shifts from stress-induced martensitic (SIM) transformation to deformation twinning ($\{332\}<113>$ type and $\{112\}<111>$ type) and to dislocation slip with increasing β phase stability. The SIM transformation results in pseudo-elasticity and enhanced ductility, but limited yield strength [3–5]. On the other hand, the $\{332\}<113>$ twinning, which usually displays higher CRSS (critical resolved shearing stress) than SIM, leads to significant strain-hardening by dynamic Hall–Petch effect by reducing the mean free path of dislocation slip in BCC grains [6]. Recently, considerable efforts have been dedicated to developing a new family of β Ti-alloys [7–11] by combining twinning and SIM effects, i.e. the hybrid TWIP/TRIP effects (TWIP: twinning-induced plasticity, TRIP: transformation-induced plasticity), that generally display low yield strength (YS), large uniform elongation and high strain-hardening rate [9]. In hybrid TRIP/TWIP Ti-alloys [7,10], the stress plateau after the elastic limit is usually related to SIM, resulting in low YS but enhancing the uniform ductility. In contrast, the β Ti-alloys whose deformation mechanism

CONTACT Fan Sun fan.sun@chimieparistech.psl.eu PSL Research University, Chimie ParisTech-CNRS, Institut de Recherche de Chimie Paris, 75005 Paris, France; Ju Li liju@mit.edu Department of Nuclear Science and Engineering and Department of Materials Science and Engineering, Massachusetts Institute of Technology, 77 Massachusetts Avenue, Cambridge, MA 02139, USA

Supplemental data for this article can be accessed here. https://doi.org/10.1080/21663831.2019.1595763

is dominated by deformation twinning (DT) and dislocation slip lead to relatively higher YS, and a stable hardening rate [6,12]. The DT mode most frequently observed in hybrid TRIP/TWIP or pure TWIP alloy is {332} type. A new design idea is to use a combination of {112} and {332} type twinning. The aim is to further strengthen this type of alloys with a better balance between stable hardening rate and ductility. The enhancement is specially targeted to avoid the difficulties of precision cold-workability and Computerized Numerical Control (CNC) machining when using TWIP/TRIP alloys with reversible SIM transformation. In this work, a moderate metastability Ti-alloy, with nominal composition Ti–18Zr–13Mo (wt%) (hereafter called Ti–18Zr–13Mo), was proposed for both complete suppression of SIM transformation and with additional solid-solution strengthening. New insights into the cooperation between dislocation slip and multimodal twinning were further investigated by *in situ* tensile electron backscatter diffraction (EBSD) technique and post-mortem transmission electron microscopy (TEM) characterization.

The Ti–18Zr–13Mo ingot was melted by the vacuum arc-melting furnace using pure Ti, Mo and Zr. The ingot was heat-treated and then cold rolled to 0.5 mm plate with about 90% thickness reduction. The processing is the same as our previous reported method [10,11,13]. The chemical composition was analysed by electron probe micro-analysis (EPMA) on a Shimadzu EPMA-8050G system, showing good chemical homogeneity with Zr-17.83%, Mo-13.05% (wt%) and Ti-balance. The tensile samples were cut from the as-rolled plate along the rolling direction. The tensile samples were then solution-treated (ST) at 1173 K for 1.8 ks using a vertical quenching tubular furnace (quartz tube) under high vacuum. Pure Ar was used to refill the quartz tube a few seconds before releasing the samples for quenching. The samples after quenching were in full beta metastable state. Uniaxial tensile tests were performed using INSTRON 5982 machine with 10 mm gauge extensometer at a strain rate of $10^{-3}\,s^{-1}$. *In situ* tensile tests were performed using a scanning electron microscope (FEG-SEM Zeiss LEO1530 operating at 20 kV) and a Micromecha machine adapted to EBSD configuration. Secondary electron (SE) imaging and EBSD mapping were recorded during the traction loading at targeted strains. The *in situ* samples (50 mm length × 2.5 mm width × 0.5 mm thickness) were pre-polished to mirror-like finishing. The EBSD data were rendered by the OIM software. The phase constitution of the pre- and post-deformation samples were analysed by X-ray diffraction (XRD) using Bruker D8 ADVANCE with Cu Kα radiation operating at 40 kV and 40 mA. TEM (JEOL 2100 microscope operating at 200 kV) was used to characterize the deformed samples. Thin foils for TEM were prepared by a twin-jet polishing technique, using a solution of 4% perchloric acid in methanol, held at about 250 K.

Figure 1(a) displays the true strain–stress curve and corresponding strain-hardening rate ($\theta \equiv d\sigma/d\varepsilon$) of Ti–18Zr–13Mo alloy, as well as the true strain–stress curve of TWIP/TRIP Ti–12Mo alloy for comparison. Our Ti–18Zr–13Mo alloy exhibits a very high YS, stable strain-hardening rate and a good ductility. The notice should be given that the YS is much improved when comparing to the TWIP/TRIP Ti-alloys, the typical Ti–12Mo for example. Compared with Ti–12Mo alloy, the true stress–strain curve of the present alloy from the elastic to plastic transition does not display a plateau arising from SIM transformation [10], suggesting a difference in deformation mechanism between the two alloys. It can be also seen from Figure 1(a) that a typical deformation process composed by the transition regime (elastic to plastic) and the uniform plastic regime on the strain-hardening rate curve. The strain-hardening rate gradually decreases in the transition regime. Plastic regime exhibits nearly stable strain-hardening behaviour. The strain-hardening behaviour of this alloy is different from the typical TWIP Ti–15Mo (wt%) alloy [6]. The uniform elongation was calculated to be 0.18 by $d\sigma/d\varepsilon = \sigma$ based on the Considère's criterion. Figure 1(b) shows an EBSD inverse pole figure (IPF) map of the as-quenched sample, displaying the recrystallized polycrystalline structure with an average grain size (GS) of 49 μm. Figure 1(c) shows the XRD profiles of as-quenched and fracture samples. Only β phase was detected after deformation, implying either SIM has not occurred or SIM was 100% reversible to beta phase after unloading at RT. The complete absence of residual martensite phase suggests the β stability of Ti–18Zr–13Mo alloy was higher than that of Ti–12Mo alloy. The increasing of beta stability might be due to the Zr addition. Zr has been characterized as a neutral element in binary Ti–Zr alloys [1], but its role in multi-element alloys is more complicated than that in the binary situation. Experimental evidence [5,11,14–16] have shown that Zr could act as a beta-stabilizer when a beta-stabilizer presented in Ti–Zr–M systems (e.g. M = Nb or Mo). In this work, the advantage of using Zr to tune the metastability of Ti–Mo system is that Zr presented a weaker stabilization effect than that of Mo, which enlarged the chemical composition range for easier control in precision. On the other hand, the solid-solution hardening effect from Zr would also be expected. The broadened β peaks indicate heavily distorted β grains after deformation.

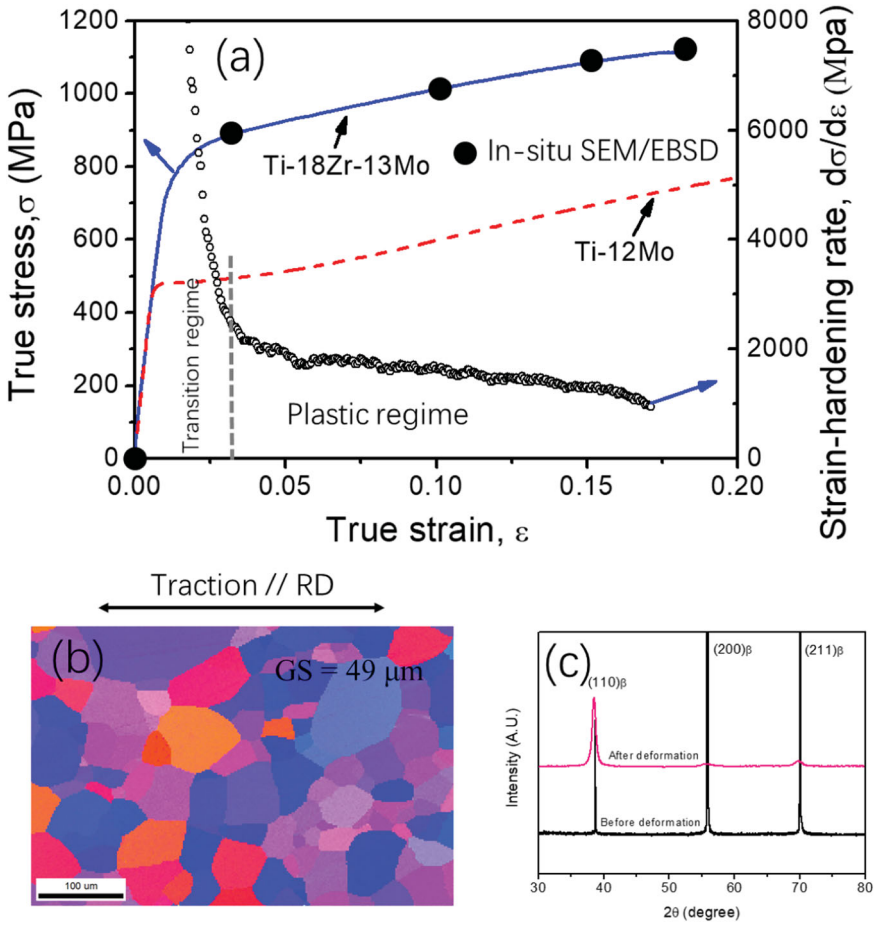

Figure 1. (a) The true strain–stress curve and corresponding strain-hardening rate of Ti–18Zr–13Mo, a Ti–12Mo curve [10] was also drawn; (b) EBSD IPF map of ST sample; (c) XRD profiles before and after deformation. A series of *in situ* SEM/EBSD mappings were made at the points ($\varepsilon = 0$, 0.03, 0.1, 0.15 and the beginning of fracture) in (a).

Figure 2(a–c) shows the sequential IPF maps taken from the same region at strain $\varepsilon = 0.03$, 0.10, 0.15 in the *in situ* SEM/EBSD straining experiments, respectively. Two variants of $\{332\} < 113 >$ twinning (332T) appeared at the micrometric scale at the beginning of the plasticity, as shown in Figure 2(a). They were labelled as 332T V1 and 332T V2. The variants form progressively a dense twinning network in the beta matrix, acting as strong barriers to reduce the mean free path of dislocation slip, i.e. the dynamic Hall–Petch effect. Upon increasing the strain to 0.10 and to 0.15, the multiplication and growth of both variants are clearly noticed in Figure 2(b,c). It is worth noting that SIM transformation was not observed during the whole plastic deformation, indicating that the TRIP effects was fully suppressed due to the higher stability of this alloy when compared with the combined TWIP and/or TRIP modes Ti-alloys [7–10,13,17]. The role of the SIM-produced α' is likely to relax the zones where strong stress concentration occurs (typically at the crossing zone of twins). Figure 2(d–f) shows the close-up details of the highlighted area in Figure 2(b,c). Note that several traces of substructure appearance were observed through the EBSD analysis. One is consistent with a classical secondary 332T occurring inside the 332T V1 region as observed in Figure 2(d). The misorientation is close to 50.5° between the 332T V1 and the secondary twinning (inset of Figure 2(d)), which corresponds to the coincidence site lattice (CSL $\Sigma 11$) theory [18], regarding the $\{332\} < 113 >$ twinning system. The other is that a grain rotation appeared at the corner of the intersection of 332T V1 and 332T V2, whose misorientation is increasing to $\sim 14°$ (inset of Figure 2(e)), was observed in Figure 2(e). Similar phenomena have reported in Ti–25Nb–0.7Ta–2Zr (at.%) alloy [12]. Yet another interesting phenomenon is that a non-conventional derivatives of the $\{5\ 8\ 11\} < 135 >$ twinning ($\{5\ 8\ 11\}$T) mode [19,20] appeared on the lower-left corner of the intersection of 332T V1 and 332T V2, as confirmed by analysis of invariant twinning plane (Figure 2(g)). This non-conventional BCC twinning mode was reported in cubic iron-nickel alloys [19,21] but is unprecedented in beta metastable Ti-alloys.

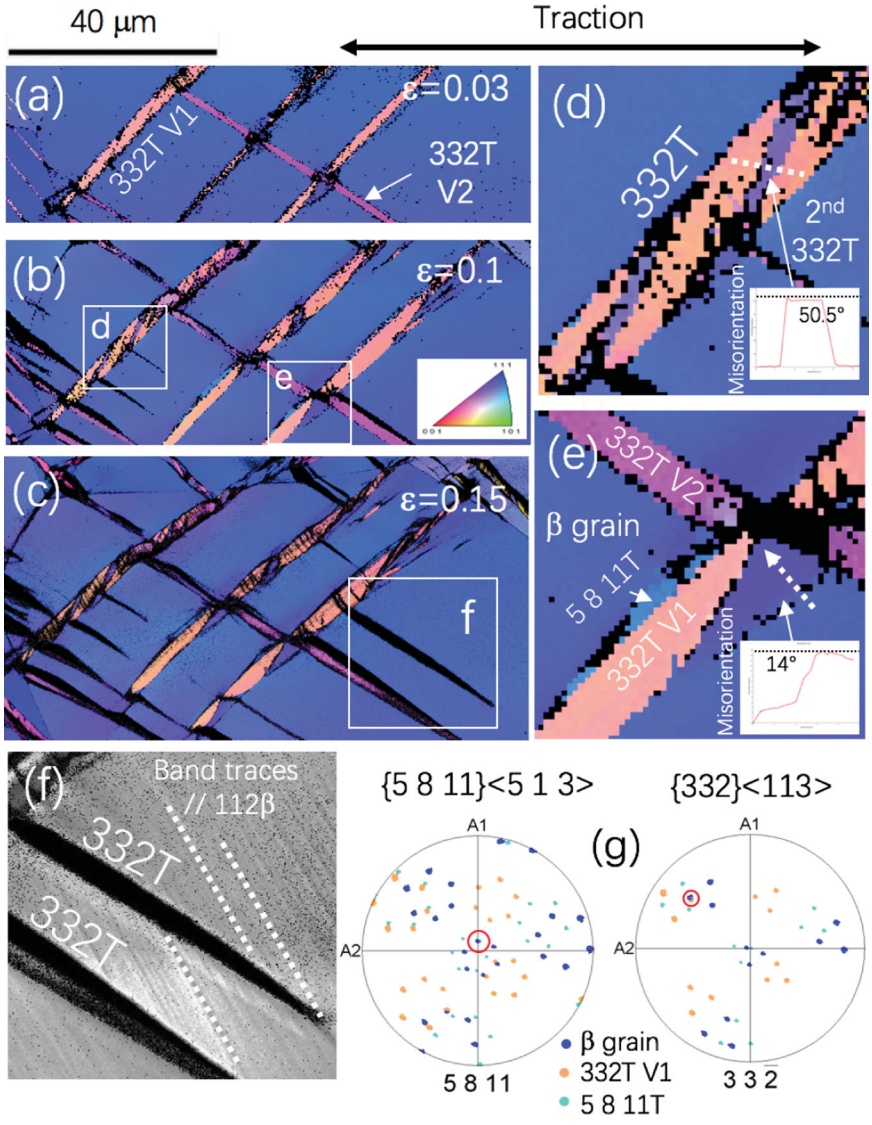

Figure 2. *In situ* EBSD mapping during traction: (a–c) EBSD IPF maps taken from the same grain at $\varepsilon = 0.03$, 0.1 and 0.15; (d–f) detailed features of (a–c); (g) pole figures of special $\{5\ 8\ 11\} < 513 >$ twinning occurred at the interface of β grain and 332T V1.

The invariant and undistorted twinning planes and shear (conjugate) directions between {5 8 11}T and β matrix were experimentally found to be $K_1 = \{5\ 8\ 11\}$, $K_2 = \{-1\ 0\ 1\}$, $\eta_1 = \{-5\ -1\ 3\}$ and $\eta_2 = \{1\ 1\ 1\}$, consistent to the theoretical prediction and the experimental observations in cubic Fe–Ni alloy [19,21]. Usually, SIM is the common mechanism to accommodate interface strain misfit [9,10,12] in TWIP/TRIP alloys. Here the SIM was completely suppressed despite the dense nano $\{112\} < 111 >$ twinning (112T) intersecting 332T (discussed below). Therefore, a plausible reason for the occurrence of {5 8 11}T is that, as Christian [20] pointed out, the {5, 8, 11}T in the cubic structure can propagate undeviated across a 112T boundary, and hence across the set of fine parallel 112Ts which are produced by the deformation. This crystallographic compatibility between {5 8 11}T and 112T might be one of the reasons that the {5 8 11}T would be the possible twinning mode to be activated near 332T interfaces, similar to the activation of relaxational martensites in TRIP/TWIP cases. Figure 2(f) shows a pair of needle-like 332Ts has nucleated at 332T V1 boundary and then propagated in the β matrix. Some thin non-indexed bands (parallel to 112 plane) are also clearly visible adjacent to the 332T V1 and 332T V2, most of them were identified to be nano 112T among {112} slip bands by further TEM analysis (described in detail in Figure 4). The width of coarse needle-like 332T deformation band tapered gradually off to a point from its initiation site to its end, which indicated the propagation of 332T deformation band may be perturbed by nano 112T. Furthermore, an additional analysis on Schmid factors (SF) is done by observing an area containing about

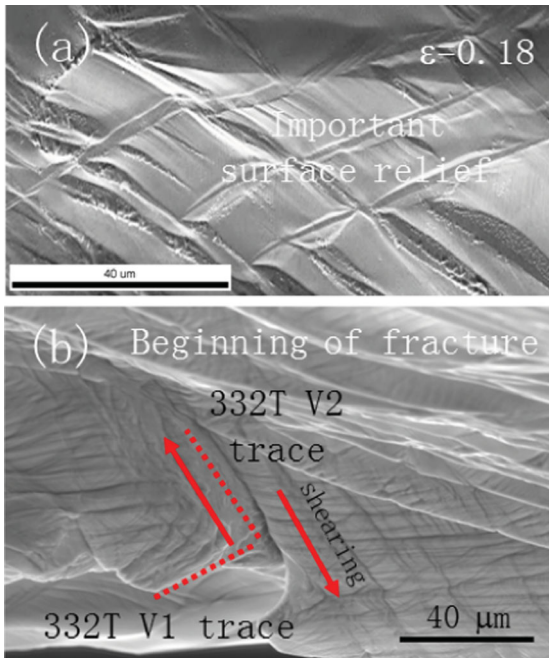

Figure 3. (a) SE images at the beginning of the fracture of the *in situ* sample: (a) important surface relief at the *in situ* area, EBSD mapping was perturbated; (b) initiation of fracture near the *in situ* area, micro-crack occurred at twinning interfaces.

80 grains on the same sample at $\varepsilon = 0.15$. The EBSD images and SF analysis of each deformation mechanisms are presented in the Supplementary Figure 1. It can be seen that 86% of the grain population exhibit quite similar SF conditions as the grain (Figure 2) studied by the *in situ* tensile EBSD. The simultaneous activation of bimodal twinning and dislocation slip would reasonably be the dominant mechanism to the polycrystalline plasticity. When close to fracture, the EBSD index confidence became weak due to strong surface relief in the *in situ* EBSD tests (Figure 3(a)). Figure 3(b) shows the SE image of the fracture surface. The deformation traces on the surface near fracture suggested that the crack initiation was probably induced by damage accumulation around localized plastic deformation taking place at the 332T boundaries. Therefore, the reduction of the uniform ductility ($\sim$20%), when comparing to 30–40% of ductility in TWIP/TRIP alloys, could probably be due to the absence of martensite relaxation near twin interfaces.

Figure 4 displays a bimodal twin structure, in which the 332Ts were tens of micrometers in thickness and are thickening during the *in situ* observation, whereas 112Ts stayed as tens of nanometers in thickness but multiplies in number. The difference in the individual variant size between 332T and 112T could be related to the magnitude of lattice shear of the two twinning modes: a 112T is 2 times higher ($s \approx 0.71$) than a 332T ($s \approx 0.35$). Thus, it is reasonable to speculate, at grain size about 50 μm, that 332T could probably be more adapted for coarsening but 112T could be probably more adapted for being thin but densely populated, as a result of the intergranular strain accommodation. It is well-known that the mechanism of 112T in BCC structure is closely related to the screw dislocation slip on the {112} plane [20]. The dissociation of $1/2 < 111 >$ dislocation occurred on the three adjacent {112} planes, forming nano-size 112T plates dispersed in parallel in the beta matrix. The nano-size 112T intersects the 332T along $< 110 >$ directions at 332T interfaces, resulting in the orientation relationship of the band-like twins observed in the micrographs (Figures 2 and 4). Obviously, the non-coplanar 112T and 332T caused competition between two mechanisms, leading to difficulties of the 332T growth, as shown in Figure 2(f) that the propagation of 332T was suppressed by 112T, preventing dangerous runaway growth that could lead to fracture. The formation of micro 332T and nano-scale 112T during plastic deformation can introduce a large amount of internal interfaces in the beta matrix and bring about continuous grain subdivision. It has been reported [12] that these interfaces, acting as barriers to dislocation motion, resulting in dynamical Hall–Petch effect. Such a persistent reduction of dislocation slip mean free path is believed to be the cause of stable strain-hardening in the present alloy.

Figure 5 shows dislocation slip occurred beside or inside 332T. The 332T was observed in Figure 5(a). The dislocations observed in Figure 5(b,c) were characterized to be the classic $1/2 < 111 >$ screw dislocations. The vectors of the imaging conditions are presented by a series of red arrows in Figure 5(b). The corresponding SAED patterns are shown in Figure 5(d–f). The in-twin line contrasts, in Figure 5(e) marked by the orange dash lines, are further explained by supplementary Figure 2. The 332T boundary and associated geometrically necessary dislocations (GND) [22] are due to a strong mechanical contrast between the twin and the matrix that may interfere with the movement of gliding dislocation, resulting in additional strain-hardening. A high density of fine-scale straight lines is observed inside the 332T, as displayed in Figure 5(c). The straight lines may act as channels for dislocation traversing, which is probably the cause of differential mobility of the lattice and twinning dislocation [20] in the matrix. From TEM observations (Figure 5 and Supplementary Figure 2), the linear contrasts observed in the 332T band were identified not to be 112T or omega phase. The lines could probably be the traces of (1–1–2) planes of the twin as dislocation channels (verified during the TEM observation, dislocations were also seen). These traces were almost aligned with the (-110) planes of the beta matrix. Since these planes were the principal gliding systems for [111] Burgers vector, it was speculated

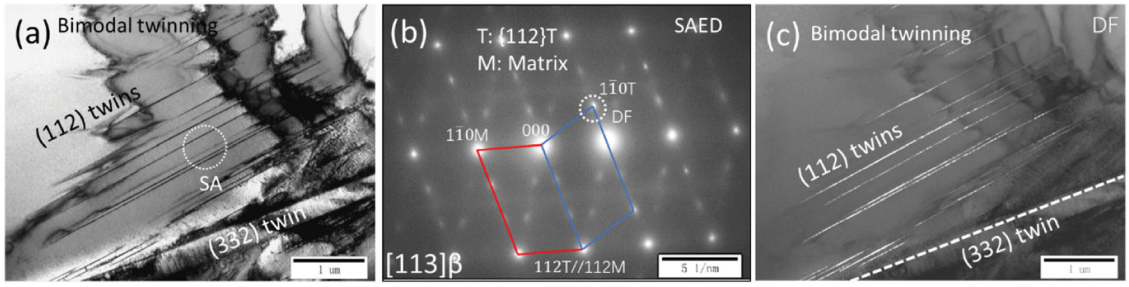

Figure 4. TEM micrographs of bimodal twinning in deformed sample ($\varepsilon = 0.03$): (a) bright field image of 112T and 332T; (b) SAED pattern along [113]β zone axis. The $1\bar{1}0$ spot of 112T can be clearly seen overlapped to one of the spots of ω variants; (c) Dark field image of 112T using marked diffraction spot (the white dotted circle) in (b).

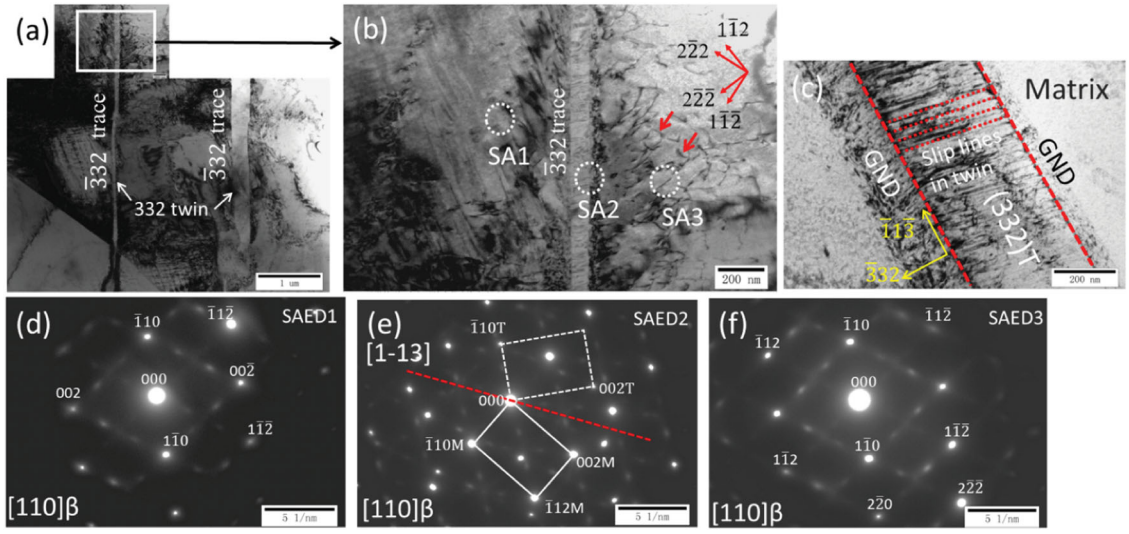

Figure 5. TEM micrographs of 332T and $1/2 < 111 >$ dislocations on the {112}β planes in deformed sample ($\varepsilon = 0.03$): (a) low-magnification bright field image of 332T; (b) bright field image of $1/2 < 111 >$ dislocations occurred near a 332T. The dislocation analysis was performed by multiple diffraction conditions to identify the dislocation type and the slip planes; (c) bright field image shows GND zones near the 332T, straight slip lines occurred inside 332T; (d–f) SAED patterns of selected area in (b).

that the interaction between the dislocations and the twin interfaces could probably one of the causes of the dislocation channelling. In addition, the pile-up of screw dislocations at different scales visualized by distinct contrast with β matrix are also observed on both sides of the 332T. Similar phenomenon has been reported in Ref. [23] that the pile-up of screw dislocations brings about a concentration of dislocations and leads to the eventual damage accumulation and fracture to initiate at the 332T boundary (Figure 3(b)). Thus, the dominant deformation mechanism could probably be the dislocation slip during the plastic flow. The direct contribution of the pure shear of crystal twinning would be quite limited to the plastic elongation when comparing to the massive dislocation slip. As evidenced by the *insitu* results, the tensile yielding of the material was accompanied by the formation of mechanical 332T and 112Ts. The critical shearing stress of the twins would probably play an important role in the yielding process. After yielding, the strain-hardening effect could probably be resulted from: (1) the dynamic reduction of the mean free path for dislocations by the growing twinning network; (2) the mechanical contrast effect between the twins and the matrix, due to the well-known strong elastic anisotropy of beta and marked by the dense network of GND at the twin/matrix interface; and (3) The progressive increase of critical stress for twinning upon loading, since this critical stress known to be closely related to the grain size (dynamically reduced during mechanical testing in TWIP alloys). Therefore, the deformation mechanism of the alloy is dominated by the activation of multimodal twinning at the early stage of plastic deformation and the subsequent complicated interaction between twinning and dislocation slip.

In summary, the newly formulated Ti–18Zr–13Mo alloy presents multimodal TWIP via the activation of multiple intersecting DT mechanisms but suppressing the occurrence of SIM transformations, which gives a better combination of strength, strain-hardening rate

and ductility. The alloy indeed exhibits extra high yield strength, stable strain-hardening rate and enough ductility. Compared with hybrid TRIP/TWIP alloys, the disappearance of TRIP effect due to enhanced β stability from the addition of 18wt% Zr contributed to the higher yield strength. The stable strain-hardening can be explained by 'dynamic Hall–Petch effect'. The appearance of a non-conventional {5 8 11} < 135 > DT mode, taking place at the twin interfaces, is likely to be a substitute for martensitic transformation to relieve the local misfit stresses generated by the {332} < 113 > and {112} < 111 > twinning systems. It is reasonable to hypothesize that the non-conventional {5 8 11}T and GND would help the ductility and strain-hardening rate. Since this is the first time {5 8 11} < 135 > are observed in TWIP Ti-alloys, its role is still not very clear, and further investigations are needed in future work.

Disclosure statement

No potential conflict of interest was reported by the authors.

Funding

This work was supported by the Fund of the State Key Laboratory of Materials Processing and Die and Mould Technology, Huazhong University of Science and Technology [grant number P2018-008]; China Postdoctoral Science Foundation [grant number 2018M632414]; National Natural Science Foundation of China [grant numbers 51601216, 51771226]; Fund of State Key Laboratory for Mechanical Behavior of Materials, Xi'an Jiaotong University [grant number 20182008].

References

[1] Lütjering G, Williams JC. Titanium. 2nd edn. Berlin: Springer; 2007.
[2] Hanada S, Izumi O. Correlation of tensile properties, deformation modes, and phase stability in commercial β-phase titanium alloys. Metall Mater Trans A. 1987;18(2):265–271.
[3] Kim HY, Ikehara Y, Kim JI, et al. Martensitic transformation, shape memory effect and superelasticity of Ti–Nb binary alloys. Acta Mater. 2006;54(9):2419–2429.
[4] Ahmed M, Wexler D, Casillas G, et al. Strain rate dependence of deformation-induced transformation and twinning in a metastable titanium alloy. Acta Mater. 2016;104:190–200.
[5] Zhang JY, Sun F, Hao YL, et al. Influence of equiatomic Zr/Nb substitution on superelastic behavior of Ti–Nb–Zr alloy. Mater Sci Eng A. 2013;563:78–85.
[6] Min X, Chen X, Emura S, et al. Mechanism of twinning-induced plasticity in β-type Ti–15Mo alloy. Scr Mater. 2013;69(5):393–396.
[7] Sun F, Zhang JY, Marteleur M, et al. A new titanium alloy with a combination of high strength, high strain hardening and improved ductility. Scr Mater. 2015;94(0):17–20.
[8] Sadeghpour S, Abbasi SM, Morakabati M, et al. A new multi-element beta titanium alloy with a high yield strength exhibiting transformation and twinning induced plasticity effects. Scr Mater. 2018;145:104–108.
[9] Gao J, Huang Y, Guan D, et al. Deformation mechanisms in a metastable beta titanium twinning induced plasticity alloy with high yield strength and high strain hardening rate. Acta Mater. 2018;152:301–314.
[10] Sun F, Zhang JY, Marteleur M, et al. Investigation of early stage deformation mechanisms in a metastable β titanium alloy showing combined twinning-induced plasticity and transformation-induced plasticity effects. Acta Mater. 2013;61(17):6406–6417.
[11] Zhang J, Li J, Chen G, et al. Fabrication and characterization of a novel β metastable Ti-Mo-Zr alloy with large ductility and improved yield strength. Mater Charact. 2018;139(139):421–427.
[12] Lai MJ, Li T, Raabe D. Ω phase acts as a switch between dislocation channeling and joint twinning- and transformation-induced plasticity in a metastable β titanium alloy. Acta Mater. 2018;151:67–77.
[13] Sun F, Zhang JY, Vermaut P, et al. Strengthening strategy for a ductile metastable β-titanium alloy using low-temperature aging. Mater Res Lett. 2017;5:547–553.
[14] Abdel-Hady M, Fuwa H, Hinoshita K, et al. Phase stability change with Zr content in β-type Ti–Nb alloys. Scr Mater. 2007;57(11):1000–1003.
[15] Hao Y, Li S, Sun S, et al. Effect of Zr and Sn on Young's modulus and superelasticity of Ti–Nb-based alloys. Mater Sci Eng A. 2006;441(1–2):112–118.
[16] Miyazaki S, Kim H, Hosoda H. Development and characterization of Ni-free Ti-base shape memory and superelastic alloys. Mater Sci Eng A. 2006:438–440:18–24.
[17] Hida M, Sukedai E, Henmi C, et al. Stress induced products and ductility due to lattice instability of β phase single crystal of Ti-Mo alloys. Acta Metall. 1982;30(8):1471–1479.
[18] Ranganathan S. On the geometry of coincidence-site lattices. Acta Crystall. 1966;21(2):197–199.
[19] Rowlands PC, Fearon EO, Bevis M. The application of the Kossel technique and electron microscopy to the study of the microstructure of Fe-32% Ni martensite crystals. J Mater Sci. 1970;5(9):769–776.
[20] Christian JW, Mahajan S. Deformation twinning. Prog Mater Sci. 1995;39(1):1–157.
[21] Fearon EO, Bevis M. The macromorphology, micromorphology, habit planes and orientation relationships associated with martensite crystals formed in a range of iron 30–34 per cent nickel alloys. Acta Metall. 1974;22(8):991–1002.
[22] Fleck NA, Ashby MF, Hutchinson JW. The role of geometrically necessary dislocations in giving material strengthening. Scr Mater. 2003;48(2):179–183.
[23] Campanelli LC, Coury FG, Guo Y, et al. The role of twinning and nano-crystalline ω phase on the fatigue behavior of the metastable β Ti–15Mo alloy. Mater Sci Eng A. 2018;729:323–330.